

Study of Sputtered Fe/t_{Si}/Fe Trilayer Films: Magnetic and Electronic Properties

Ranjeet Brajpuria^{1*}, Ram Kripal Sharma¹, Ankush Vij², T. Shripathi³

¹AMITY School of Engineering and Technology, AMITY University Haryana, Gurgaon, India

²Nano-Analysis Center, Korea Institute of Science and Technology, Seoul, South Korea

³UGC-DAE Consortium for Scientific Research, University Campus, Indore, India

E-mail: *ranjeetbjp@yahoo.co.in

Received March 21, 2011; revised April 29, 2011; accepted May 11, 2011

Abstract

A series of trilayers of sputtered Fe/Si/Fe were grown to study the interface characteristics and magnetic coupling between ferromagnetic Fe layers (30 Å thick) for Si spacer thickness (t_{Si}) ranging from 15 Å to 40 Å. Grazing incidence x-ray diffraction, AFM, resistivity and x-ray photoelectron spectroscopy (XPS) measurements show substantial intermixing between the layers during deposition which results in trilayers of complicated structures for different sub-layer thicknesses. A systematic variation in silicide concentration across the interface is observed by XPS measurements. The Fe layers in the trilayers were observed to consist of Fe layers doped with Si, ferromagnetic Fe-Si silicide layers and nonmagnetic Fe-Si silicide interface layer, while the Si spacer was found to be Fe-Si compound layers with an additional amorphous Si (α -Si) sublayer for t_{Si} ≥ 30 Å. A strong anti-ferromagnetic (AF) coupling was observed in trilayers with iron silicide spacers, which disappeared if α -Si layers present in the spacers. The observed magnetization behaviour in each case is interpreted in terms of changes in interfacial structural and electronic properties due to variation in film thickness.

Keywords: Magnetic Multilayer, Silicide Formation, Interlayer Coupling, MOKE, XPS

1. Introduction

With the ever-rising demands on thin film technology, understanding and controlling thin film growth is vital particularly in case of giant magnetoresistive (GMR) sensors. The strength of the antiferromagnetic coupling depends on the interfacial structure, which in turn depends on the growth of the material. After the first report of antiferromagnetic (AF) coupling between Fe films spaced by Cr in Fe-Cr-Fe sandwiches [1], a number of studies demonstrated that long range coupling between two ferromagnets separated by non-magnetic transition metals or noble metals was a fairly general phenomenon with oscillatory character and short and long periods [2-5]. The coupling mechanism is thought to be induced by the polarization of conduction electrons in the spacer layer via a Ruderman-Kittel-Kasuya-Yoshida (RKKY) like interaction [6]. A spin-dependent Quantum well description of the electronic structure has also been proposed [7,8]. All of these models share in common the occurrence of a periodic exchange coupling as a result of

two intrinsic properties of the spacer materials: the existence and topology of the fermi surface and the discreteness of the layer thickness.

Although present theories describe coupling in systems with metallic spacers, it is not clear how these theories can be extended to explain coupling across non-metallic spacers. The mechanism of interlayer coupling across a semiconducting spacer layer could be fundamentally different from that observed for ferromagnetic films, coupled across nonmagnetic metallic spacer layers. Recently, it was discovered that sputtered and evaporated Fe/Si/Fe trilayers [9,10] and Fe/Si multilayers [11] exhibit AF coupling. The spacers inducing AF coupling are different in two cases. AF coupling in the multilayers was observed only for crystalline spacer layers, attributed to iron silicide formed at the interface, whereas in the trilayers, the spacer was claimed to be amorphous semiconducting Si. The interpretation of the coupling data has been hampered by lack of knowledge about the spontaneously formed iron silicide layer at the interfaces, which has been variously hypothesized to be a metallic

compound in the B2 structure or a semiconductor in the more complex B20 structure [12,13]. In general, severe interdiffusion occurs at Fe/Si interfaces, resulting in the formation of various kinds of silicides [14]. Consequently, the interaction of ferromagnetic layers across different silicides may show antiferromagnetic or ferromagnetic coupling depending on the kind of silicide.

Although a number of experimental works have been done to understand the mechanism of interlayer coupling in this system, the results are controversial and it is not yet well understood how the formation of iron silicide in the spacer layer affects the coupling. In order to understand the mechanism of the coupling in these multilayers, it is of central importance to elucidate the chemical and magnetic properties of the spacer layer. Studies have dealt with the Fe/Si (100) interface at room temperature [15-23] and several of these studies included photoemission measurements [19-22]. Different estimates of the thickness of reacted layer at the interface have been made ranging from 0 Å to ~30 Å [15,17-19,21]. Also the chemical composition of the interface layer is still a disputed question. Various silicides like FeSi [17], FeSi₂ [16,18] and Fe₃Si [20,21] have been proposed to form at the Fe/Si (100) interface. Up to now very little is known about the correlation between interface chemistry and magnetism. Therefore, in order to investigate this correlation we have synthesized [Fe (30 Å)/t_{Si}/Fe (30 Å)] trilayers samples using ion beam sputtering system and studied these properties as a function of Si layer (where, t_{Si} = 15 Å - 40 Å) thickness.

2. Experimental Details

An Ion beam sputtering (IBS) system with a Kaufman type ion source was used to prepare the Fe/Si/Fe trilayer samples in the present study. The system base pressure was 2×10^{-8} Torr. The Ar⁺ ions are incident at an angle of about 45° on the planar targets of Fe and Si with purity higher than 99.99% at 1000 V. Prior to deposition, ex-situ cleaning of the substrates was done using the following method. The glass substrates were initially washed with soap solution and rinsed with distilled water. Before loading to UHV chamber, they were dried using infrared lamp. Deposition rates for Fe and Si were 32 Å and 52 Å/min, respectively. The Fe layer thickness was fixed to 30 Å and the thickness of Si layer was varied in the range of 15 Å to 40 Å.

Grazing incidence x-ray diffraction (GIXRD) measurements were done using Cu x-ray source ($\lambda = 1.542$ Å) operated at 40 KV and 30 mA. Atomic force microscopy (AFM) measurements were carried out in the contact mode in air using Digital Instruments Nanoscope III. The images were recorded immediately after removing the

samples from the deposition system so as to minimize contamination to the samples. Different portions of each film were scanned in order to get global information of the sample. The images were acquired on areas varying from $5 \mu\text{m} \times 5 \mu\text{m}$ to $1 \mu\text{m} \times 1 \mu\text{m}$ with a 256×256 pixel array.

The associated changes in magnetic properties were characterized by means of magneto optical Kerr effect (MOKE) technique with a laser source (He-Ne) of wavelength 6328 Å. The corresponding transport properties were obtained by employing four-probe resistivity method. X-ray photoelectron spectroscopy (XPS) study was carried out using OMICRON EA-125 photoelectron spectrometer at a base pressure better than 5×10^{-10} Torr. The spectra were collected using Mg K_α radiation and the overall energy resolution was about 0.8 eV. Au 4f_{7/2} at 84.7 eV binding energy (B.E) served as an external and C-1s as an internal reference. In order to avoid any charging effect, proper grounding had been made. The Ar⁺ ions energies up to 1.5 KeV were used to avoid surface damage and intermixing during etching. The energy scale was calibrated using the Fermi level and the peak positions from the system database. The spectra were normalized to the maximum intensity after a constant background subtraction. All the measurements reported in this paper were carried out at room temperature.

3. Results and Discussion

3.1. Grazing Incidence X-Ray Diffraction (GIXRD) and AFM Measurements

Magnetic properties are strongly dependent on crystal structure of the material. Thus, the crystal properties of these trilayers films were analyzed in order to identify the causes of the variation in magnetic properties.

Figure 1 shows the GIXRD patterns of as-deposited [Fe (30 Å)/Si (15 Å - 30 Å)/Fe (30 Å)] trilayer samples. All the patterns exhibited only single peak and it corresponds to the diffraction from α -Fe (110). The absence of any Si peak indicates the amorphous nature of deposited Si film in all the cases. However, the peak corresponding to α -Fe (110) of trilayer samples was significantly different from that of bulk Fe. We interpret that the peak position shift is caused by the elongation of the (110) interplanar distance 'd' due to large internal stress in the Fe layers induced by adjacent Si layers, and their intermixing during deposition causing the formation of iron silicide layer at the interface. Further, the intensity of (110) peak reduces substantially and FWHM increases with increasing Si layer thickness. Particularly for Si ≥ 30 Å, the peak shows a broad hump around $2\theta = 43.56^\circ$, due to further growth of iron silicide layer along with appearance of an amorphous Si (α -Si) layer at the interface.

Figure 2 shows the t_{Si} dependence of particle size and

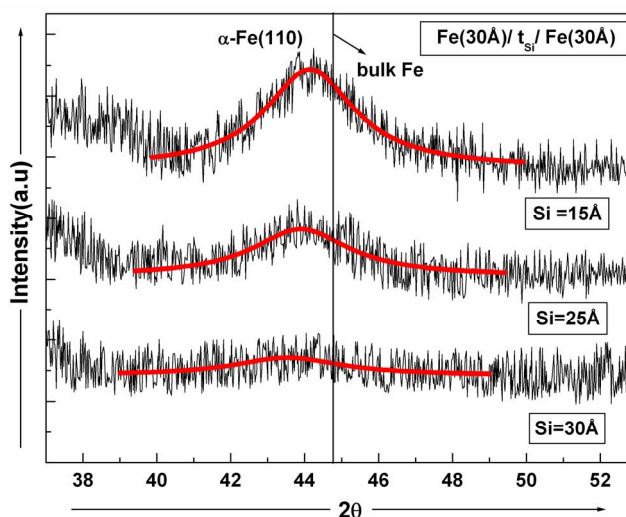


Figure 1. GIXRD patterns of as-deposited [Fe(30 Å)/Si(15 Å - 30 Å)/Fe(30 Å)] trilayer samples.

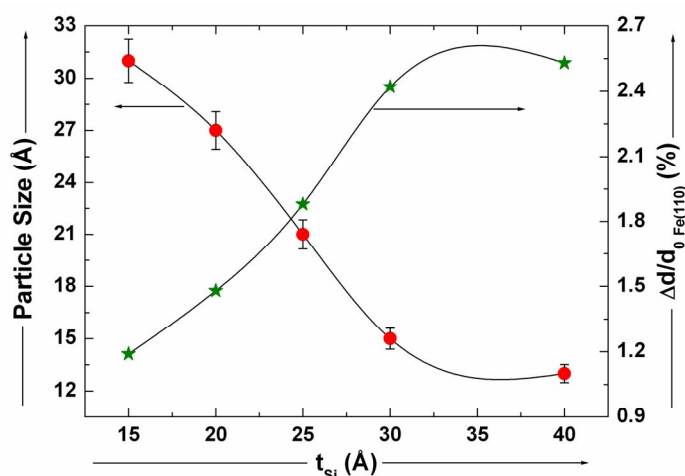


Figure 2. The dependence of particle size and elongation in interplanar distance of α -Fe(110) $\Delta d/d_0$ on t_{Si} .

elongation in the interplanar distance of α -Fe (110), $\Delta d/d_0$, in the trilayer samples evaluated from the GIXRD patterns as shown in **Figure 1**. Here d_0 denotes the (110) interplanar distance of bulk α -Fe crystallites with a perfectly cubic lattice and Δd denotes the difference between the (110) interplanar distance, d , of the trilayers and d_0 . The particle size obtained from Scherrer formulism decreases substantially with increasing t_{Si} , indicating that trilayers with smaller t_{Si} have larger and more oriented α -Fe (110) crystallites and t_{Si} beyond 25 Å appeared to be composed of micro-crystallites or amorphous Fe grains, which we assume, are due to the appearance of pure amorphous Si (α -Si) layer in the spacer. On the other hand, $\Delta d/d_0$ increase monotonically with increase of t_{Si} and saturated at about 2.42% for $t_{Si} > 25$ Å. This suggests that the elongation may be attributed to the large compressive stress in the Fe layers imposed by adjacent Si layer.

The quality of surface and interface structure plays decisive role in achieving optimum performance for which the multilayer structure is designed. Therefore, further information about the structure and surface morphology can be obtained from AFM studies conducted on Fe/Si/Fe trilayer samples. **Figure 3** shows the three-dimensional AFM images of [Fe (30 Å)/Si (15 Å)/Fe (30 Å)] and [Fe (30 Å)/Si (30 Å)/Fe (30 Å)] trilayer samples obtained from $2 \times 2 \mu\text{m}^2$ sample area using contact mode. It is clearly seen from **Figure 3(a)** that the deposited layers are nearly continuous showing a valley like features with wide distribution of the sizes and separation, giving rise to a very large rms surface roughness value. These valleys like features are clearly indicating the crystalline and oriented growth of Fe. However, as the thickness of Si layer increases to 30 Å (see **Figure 3(b)**), the separation of these features decreases and show the formation of more continuous and denser layers compared

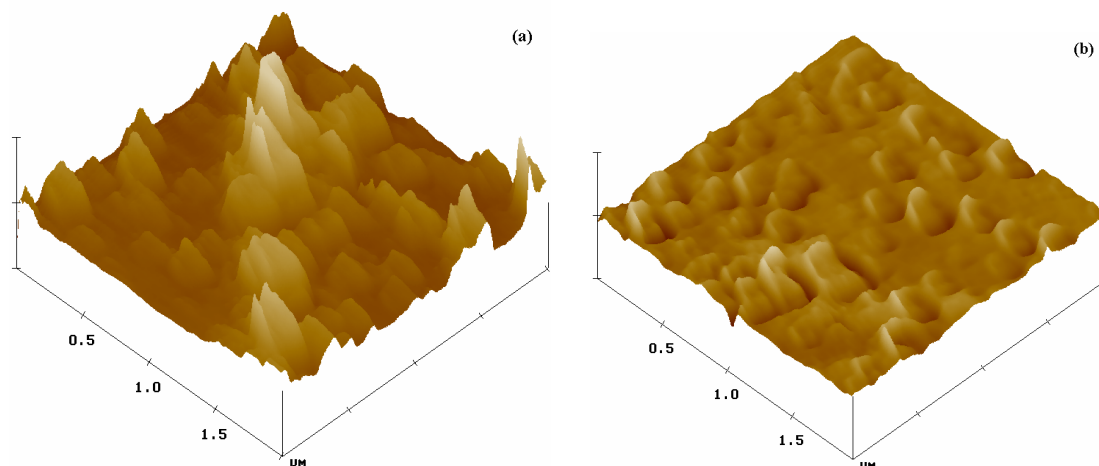


Figure 3. Three-dimensional AFM images of (a) [Fe(30 Å)/Si(15 Å)/Fe(30 Å)] and (b) [Fe(30 Å)/Si(15Å)/Fe(30 Å)] triayer samples.

to the above-mentioned case, which is due to the appearance of pure amorphous Si (α -Si) layer in the spacer and as a result the value of surface roughness decreases. This is in correlation with the XRD data's. Hence, the obtained AFM pictures provide us more clear information about different growth stages, as the Si layer thickness is increased from 15 Å to 40 Å.

3.2. Magneto-Optical Kerr Effect (MOKE) Measurements

In order to see the variation in AF coupling with increasing spacer layer thickness t_{Si} , MOKE measurements have been performed. For all the samples, magnetic field was applied parallel to the surface of the film and hysteresis loops were recorded upto the saturation magnetization. **Figure 4** shows the evolution of MOKE loops for Fe/Si/Fe trilayer samples as a function of Si layer thickness. As can be seen, the magnetic parameters like the remanent (M_R) to saturation (M_S) magnetization ratio (the so-called $F_{AF} = 1 - M_R/M_S$ parameter) and saturation field (H_S) are strongly influenced by the spacer thickness. In metallic MLS the F_{AF} parameter is usually treated as proportional to the AF coupled fraction of the sample, and $F_{AF} = 1$ when ML is completely AF coupled and $F_{AF} = 0$ for a ferromagnetically coupled MLS.

Figure 5 displays the values of F_{AF} and the saturation field (H_S) for the Fe/Si/Fe trilayer samples as a function of spacer layer thickness t_{Si} . F_{AF} dependence shows that the strong AF coupling occurs at $t_{Si} = 25$ Å where $F_{AF} = 0.38$. Similar dependence and occurrence of only single maximum of F_{AF} are reproduced by H_S (t_{Si}). For $t_{Si} = 25$ Å, H_S reaches its maximum value of about 158 Oe, which may also indicate the occurrence of a very strong AF interlayer coupling. For $t_{Si} > 25$ Å, both F_{AF} and H_S

values are strongly reduced, $F_{AF} < 0.1$ and $H_S < 90$ Oe. The reduction of F_{AF} and H_S values for $t_{Si} < 25$ Å points out that the neighbouring Fe layers become gradually connected through pinholes. However, it is noted that the rate of change of AF coupling with spacer layer thickness on both sides of the AF peak is not the same. The difference is mainly due to changes in interlayer structure according to different sub-layer thicknesses.

From **Figure 4** one can see the existence of different interlayer coupling that modifies the shapes of hysteresis loops from square-like to step-like. For $t_{Si} = 15$ Å, the hysteresis loop is square in shape indicating that the distribution of anisotropy is rather sharp which makes the domain magnetization switching beyond certain applied magnetic field. The large vertical jump with retentivity almost equal to saturation magnetization and lower coercivity value suggest the soft magnetic behaviour of the sample with strong anisotropy leading to in plane easy direction of magnetization. However, shape of the hysteresis loop changes from square to smoother one as the spacer layer thickness increases to $t_{Si} = 25$ Å, indicating strong AF coupling at this thickness. Further on increasing the thickness of spacer layer from 25 Å to 30 Å and 40 Å, shape of the loop again changes to step-like, characterized by two "coercive" fields: H_{C1} and H_{C2} , indicating the presence of different phases at these thicknesses. This peculiar behaviour is mainly due to the presence of silicide layer along with pure α -Si layer at the interface. Due to weak coupling the correct identification of the saturation fields is very difficult. Therefore, in the inset of **Figure 5**, we also present the values of H_{C1} and H_{C2} fields as a function of spacer thickness. From the figure, one can see that H_{C2} appears only for thicker Si layer, *i.e.*, for $t_{Si} \geq 30$ Å. Hence, above magnetic measurements conclude that Fe layers in the trilayers generally consist of Fe layers doped

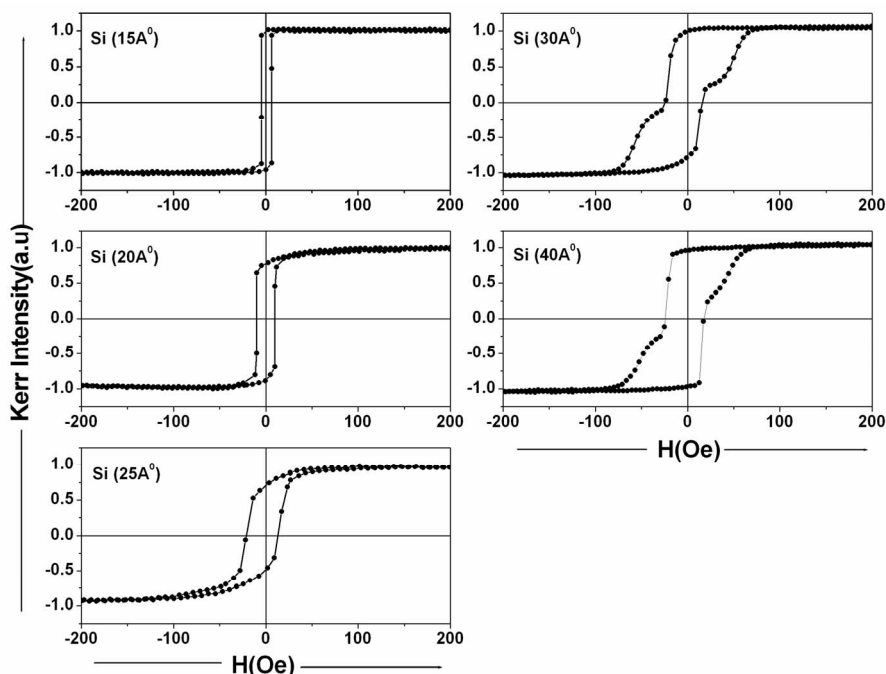


Figure 4. Hysteresis loops of as-deposited [Fe(30 Å)/Si(15 Å–40 Å)/Fe(30 Å)] trilayer samples.

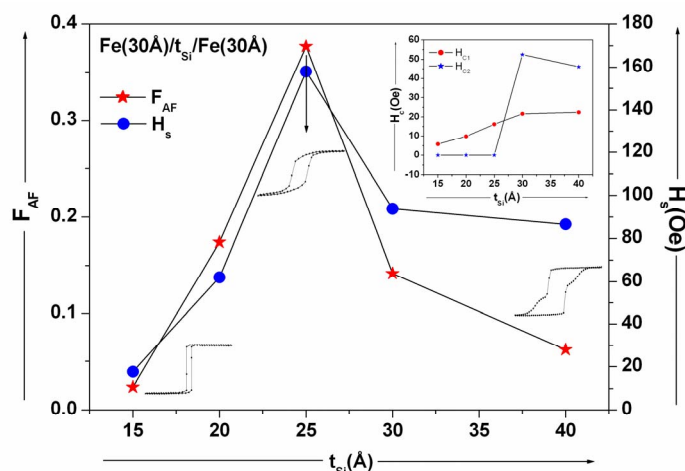


Figure 5. Dependence of F_{AF} and H_s on spacer thickness. Inset shows the variation in coercivity with spacer thickness.

with Si, ferromagnetic Fe-Si silicide layers and nonmagnetic Fe-Si silicide interface layers, while the nominal Si spacers turn out to be Fe-Si compound layers with additional α -Si sublayers only under the condition where $t_{Si} \geq 30$ Å. A strong AF coupling is observed with iron silicide spacers and disappears when α -Si layers appear in the spacer.

3.3. X-Ray Photoelectron Spectroscopy (XPS) Measurements

In order to further investigate the chemical nature of layers at surface and interface in the as-deposited Fe/Si/Fe

trilayer samples, XPS measurements have been performed after repeated sputtering of sample surface by Ar^+ ions. This gave the chemical composition of the film at different depths, averaged over the escape depth of photoelectrons (~ 40 Å). The interfaces are analyzed when the top layer was Fe or Si rich and also when top layer was Si (Si/Fe interface). It was performed on purpose to note the possibility of inequivalence of the interfaces, as an AES study by Strijkers *et al.* indicated some differences of interfaces at iron silicide formation [24].

Figure 6 shows the survey scans of as-deposited sample surface of Fe(30 Å)/Si(15 Å)/Fe(30 Å) trilayer before and after 10 min sputtering. From the spectrum (before

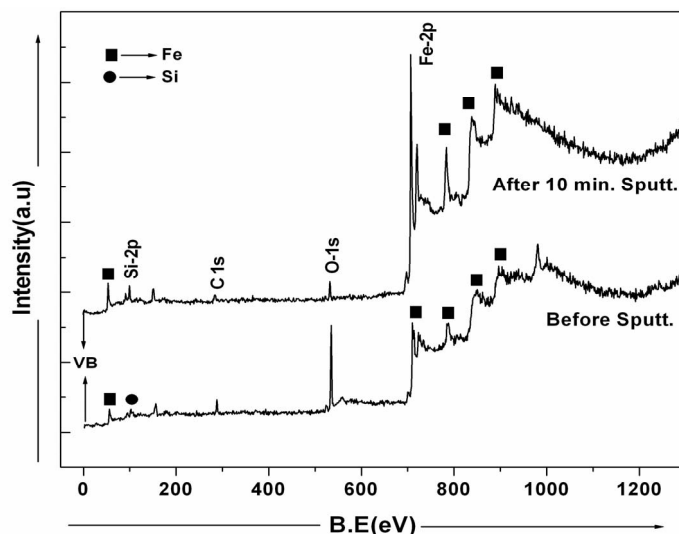


Figure 6. XPS survey scans of [Fe(30 Å)/Si(15 Å)/Fe(30 Å)] trilayer sample before and after sputtering.

sputtering) one can see that peaks corresponding to carbon (C), oxygen (O) and iron (Fe) are clearly visible, whereas very small contribution due to silicon (Si) is observed. This small presence of Si peaks is expected, as Si is the second layer after Fe (30 Å) top layer. Since the sample was exposed to air, there are large quantities of absorbed carbon and oxygen on the surface as evident from the spectrum. However after sputtering the sample for 10 min, the intensity of carbon and oxygen drops to minimum with appearance of buried Si peaks, indicating that signals are coming from the first interface region. We also note that the reduction in the carbon content is more rapid than oxygen content and may be attributed to preferential sputtering of carbon with respect to reacted oxygen.

Figure 7 shows the fitted (a) Fe-2p and (b) Si-2p core level spectra of Fe(30 Å)/Si(15 Å)/Fe(30 Å) trilayer sample as a function of sputtering time. For comparison, core levels from clean Fe and Si single layer films are also given in the same figure. We note that these spectra are in excellent agreement with previous reports [25]. Before sputtering the observed spectrum of Fe presents significant differences, which are characteristic of the oxidized state. Fe-2p_{3/2} peak is shifted to binding energy (B.E) of 710.5 eV by the change in electrostatic potential at the Fe sites. This chemical shift is caused by the partial transfer of electrons from the Fe³⁺ to the O²⁻ ions. The 2p_{3/2} peak is broadened by multiplet splitting involving the core hole and the valence electrons. Finally, the 2p_{3/2} peak shows a distinct satellite feature around 714.6 eV B.E, caused by charge-transfer processes. The main peak corresponds to so-called well-screened 2p³3d⁶L final state configuration, while the satellite corresponds to so-called poorly screened 2p⁵3d⁵ final state configuration (L denotes a ligand hole) [26]. However after sputtering for 5

min, the presence of sharp peak around 707.0 eV and tail towards higher B.E indicates that signals are coming mostly from elemental Fe region. The spectra are split by the 2p spin-orbit effect into the 2p_{3/2} and 2p_{1/2} regions and continuous tail is caused by the electron-hole pair excitations and is a significance of metallic states. However, this peak is shifted by 0.2 eV towards higher B.E as compared to clean Fe-2p core level. This shift indicates the formation of iron silicide (FeSi) layer at the interface in as deposited trilayer sample. Similarly, after 10 min sputtering, it is observed that this peak is further shifted by 0.1 eV towards higher B.E of 707.1 eV, suggesting that signals are now coming mostly from the first interface region *i.e.*, more from silicide layer. However after further sputtering the sample for 15 min, no noticeable changes are observed in the B.E and FWHM of this peak.

Similarly, figure. 7b shows the Si-2p core level spectra of Fe(30 Å)/Si(15 Å)/Fe(30 Å) trilayer sample with respect to sputtering time. In this case, before sputtering peaks due to Si are very small in intensity as it is the second layer after 30 Å top Fe layer as discussed earlier. However, after 5 min sputtering, spectrum clearly shows the presence of buried Si-2p peaks. A closer inspection of this peak shows small presence of SiO₂ peak along with elemental Si-2p (99.7 eV) peak at a B.E position of 102.1 eV. The set of typical Si-2p spectra consist of spin orbit doublet peaks corresponding to Si-2p_{3/2} and Si-2p_{1/2} level states. However, spectrometer resolution does not allow distinction of their structure. Similar to the case of Fe-2p after 5 min sputtering, Si-2p peak is also found to be shifted by 0.2 eV towards higher B.E as compared to elemental Si-2p further suggesting the formation of silicide layer at the interface. Upon further sputtering the sample for 10 and 15 min, there are no changes (B.E and

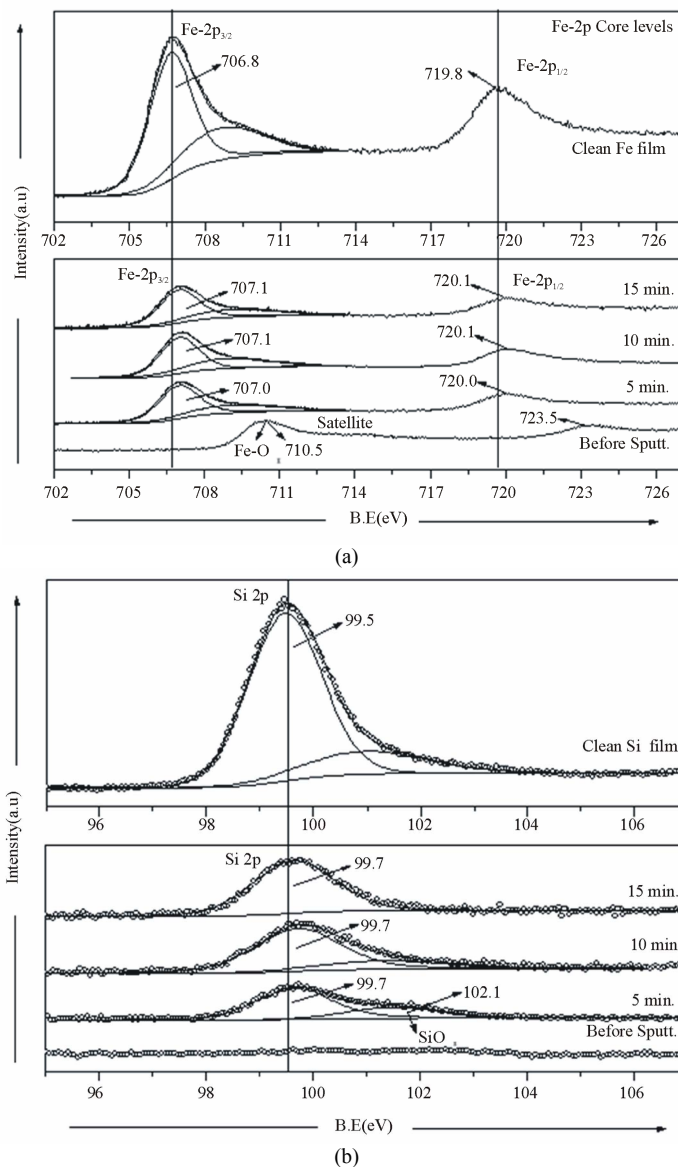


Figure 7. (a) Fe-2p and (b) Si-2p core level spectra of [Fe(30 Å)/Si(15 Å)/Fe(30 Å)] trilayer sample as a function of sputtering time.

and FWHM values) in the Si-2p spectra. The above results show that there seems to be no changes in the core level spectra of both Fe-2p and Si-2p with respect to sputtering, suggesting that silicide layer is formed at the interfaces during deposition and also complete Si layer is interdiffused into Fe layers thereby converting as deposited Fe/Si/Fe trilayer structure to Fe/FeSi/SiFe/Fe structure.

Figure 8 shows the fitted (a) Fe-2p and (b) Si-2p core level spectra of Fe(30 Å)/Si(40 Å)/Fe(30 Å) trilayer sample with respect to sputtering time. In this case also, before sputtering, the surface is completely oxidised and the spectrum mostly shows oxidised states of Fe-2p core levels. After 5 min sputtering, similar to earlier case,

Fe-2p and Si-2p core levels are shifted by 0.3 eV and 0.2 eV respectively towards higher B.E as compared to core levels of pure Fe and Si layers, suggesting the formation of silicide layer at the interface. After further sputtering for 5 min (total 10 min) a drop in the Fe-2p and increment in the Si-2p core level intensities is observed. Apart from this, no shift is observed in the B.E position of Fe-2p core level, whereas slight shifts of 0.1 eV towards lower B.E (99.6 eV) is observed in case of Si-2p core level. Upon further sputtering for 5 min (total 15 min) one can clearly see more reduction in Fe-2p with observable enhancement in Si-2p core level intensity. However, an important point to be noticed here is that Si-2p core level is further shifted by 0.1 eV towards

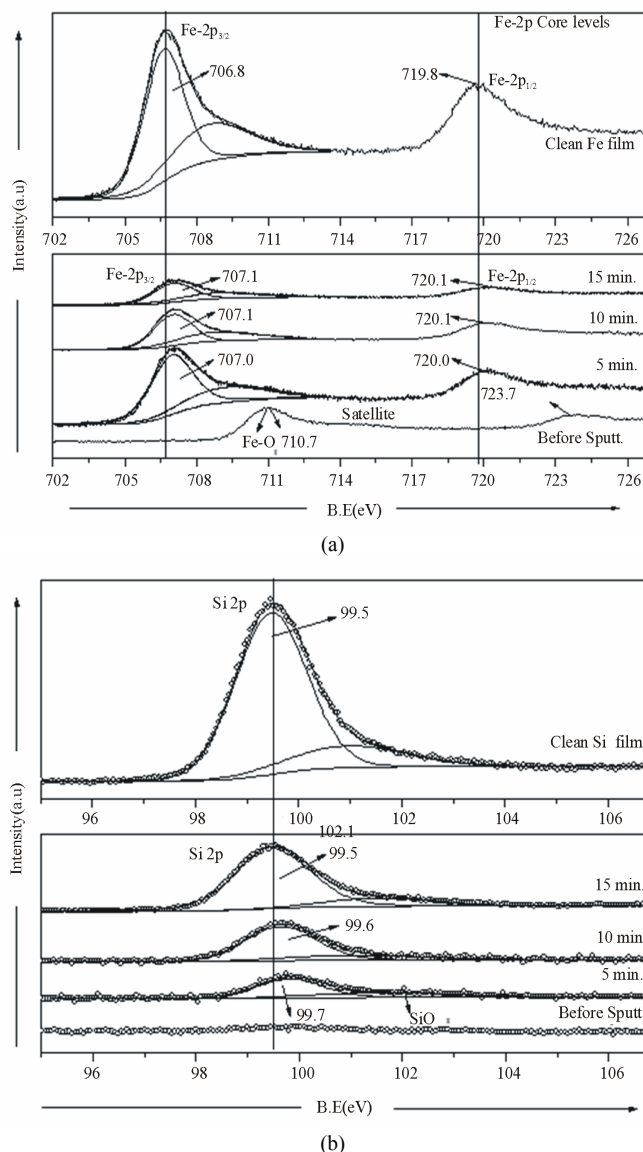


Figure 8. (a) Fe-2p and (b) Si-2p core level spectra of [Fe(30 Å)/Si(40 Å)/Fe(30 Å)] trilayer sample as a function of sputtering time.

lower B.E (99.5 eV), and still no shift is found in the B.E of Fe-2p core level. The shift only in Si-2p core level towards clean Si-2p core level indicates the appearance of elemental Si layer at this situation and still small presence of silicide layer from the first interface causes Fe-2p core level to remain shifted.

Based on the above-mentioned XRD, MOKE and XPS results we have proposed a model for Fe/Si/Fe trilayer sample having the Si layer thickness 15 Å and 40 Å, respectively as shown in **Figure 9**. The model shows the formation of silicide layer at the interfaces in both the cases. However, apart from silicide layer, pure α -Si layer is also observed only in case of [Fe(30 Å)/Si(40 Å)/Fe(30 Å)] trilayer sample.

3.4. Resistivity Measurements

Figure 10 shows the variation of the resistivity (ρ) versus nominal Si layer thickness t_{Si} at room temperature. It is shown that the resistivity increases slowly with increasing t_{Si} for the films with $t_{Si} < 25$ Å. Near $t_{Si} \geq 25$ Å, the resistivity increases rapidly, and when $t_{Si} > 30$ Å it is nearly constant with a slightly increasing tendency. The t_{Si} dependence of the resistivity in this system is quite peculiar and different from many metallic multilayered systems [27]. It is known that FeSi silicide is easily formed at the interface due to atomic intermixing and interdiffusion and the resistivity of FeSi silicide is much higher than the resistivity of Fe [28]. Thus peculiar t_{Si} dependence of the

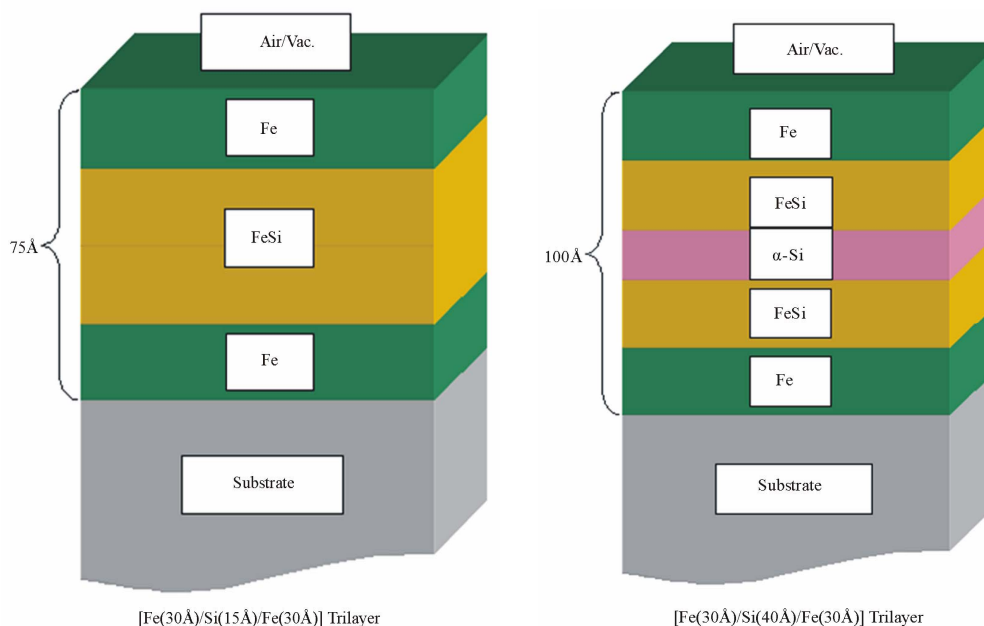


Figure 9. Schematic representation of the trilayer samples having Si layer thickness $t_{\text{Si}} = 15 \text{ \AA}$ and 40 \AA .

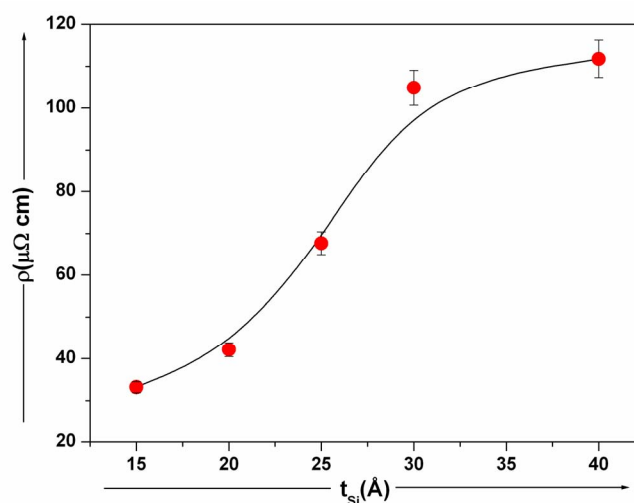


Figure 10. Variation of resistivity as a function of spacer thickness.

resistivity for $t_{\text{Si}} < 25 \text{ \AA}$ can be explained as mainly due to the increase of interdiffusion and the silicide formation with increasing t_{Si} . The rapid increase of the resistivity and changes in GIXRD and MOKE data at $t_{\text{Si}} \geq 25 \text{ \AA}$ can be understood by that in addition to the FeSi layer, a α -Si layer appears in the spacer as also revealed from our XPS results. The appearance of α -Si layer in the spacer stops further interdiffusion and results in no appreciable change in the resistivity and also prevents AF coupling after $t_{\text{Si}} \geq 30 \text{ \AA}$.

4. Conclusions

The structural, magnetic and transport properties of sput-

tered Fe/Si/Fe trilayers were studied as a function of Si spacer thicknesses. The GIXRD, MOKE, resistivity and XPS measurements demonstrate that in addition to the iron silicide at Fe/Si interface an α -Si layer begins to appear in the spacer when $t_{\text{Si}} \geq 30 \text{ \AA}$. The Fe layers in the trilayers were observed to consist of Fe layers doped with Si, ferro-magnetically ordered Fe-Si silicide layer, and nonmagnetic iron silicide dead layers at the interface. A strong AF coupling is observed with iron silicide spacer and disappears when α -Si layer appears in the spacer.

5. Acknowledgements

The authors would like to acknowledge Prof. A. Gupta

for MOKE measurement. Special thanks are due to the help provided by S. Sengar in collecting data. The help rendered by Mr. A. Wadiker in XPS measurements and Mr. S. Potdar in depositing the samples is also acknowledged.

6. References

- [1] P. Grunberg, R. Schreiber, Y. Pang, M. B. Brodsky and C. H. Sowers, "Layered Magnetic Structures: Evidence for Antiferromagnetic Coupling of Fe Layers across Cr Interlayers," *Physical Review Letters*, Vol. 57, No. 19, 1986, pp. 2442-2445. [doi:10.1103/PhysRevLett.57.2442](https://doi.org/10.1103/PhysRevLett.57.2442)
- [2] S. S. P. Parkin, "Systematic Variation of the Strength and Oscillation Period of Indirect Magnetic Exchange Coupling through the 3d, 4d, and 5d Transition Metals," *Physical Review Letters*, Vol. 67, No. 17, 1991, pp. 3598-3601. [doi:10.1103/PhysRevLett.67.3598](https://doi.org/10.1103/PhysRevLett.67.3598)
- [3] M. T. Johnson, S. T. Purcell, N. W. E. McGee, R. Coerhoon, J. Van de Stegge and W. Hoving, "Structural Dependence of the Oscillatory Exchange Interaction across Cu Layers," *Physical Review Letters*, Vol. 68, No. 17, 1992, pp. 2688-2691. [doi:10.1103/PhysRevLett.68.2688](https://doi.org/10.1103/PhysRevLett.68.2688)
- [4] J. Unguris, R. J. Cellota and D. T. Pierce, "Observation of Two Different Oscillation Periods in the Exchange Coupling of Fe/Cr/Fe(100)," *Physical Review Letters*, Vol. 67, No. 1, 1991, pp. 140-143. [doi:10.1103/PhysRevLett.67.140](https://doi.org/10.1103/PhysRevLett.67.140)
- [5] S. N. Okuno and K. Inomata, "Dependence on Fermi surface Dimensions of Oscillatory Exchange Coupling in Co/Cu_{1-x}Ni_x(110) Multilayers," *Physical Review Letters*, Vol. 70, No. 11, 1993, pp. 1711-1714. [doi:10.1103/PhysRevLett.70.1711](https://doi.org/10.1103/PhysRevLett.70.1711)
- [6] P. Bruno and C. Chappert, "Oscillatory Coupling between Ferromagnetic Layers Separated by a Non-magnetic Metal Spacer," *Physical Review Letters*, Vol. 67, No. 12, 1991, pp. 1602-1605. [doi:10.1103/PhysRevLett.67.1602](https://doi.org/10.1103/PhysRevLett.67.1602)
- [7] D. M. Edwards, J. Mathon, R. B. Muniz and M. S. Phan, "Oscillations of the Exchange in Magnetic Multilayers as an Analog of de Haas-van Alphen Effect," *Physical Review Letters*, Vol. 67, No. 4, 1991, pp. 493-496. [doi:10.1103/PhysRevLett.67.493](https://doi.org/10.1103/PhysRevLett.67.493)
- [8] J. E. Ortega and J. Himpfel, "Quantum Well States as Mediators of Magnetic Coupling in Superlattices," *Physical Review Letters*, Vol. 69, No. 5, 1992, pp. 844-847. [doi:10.1103/PhysRevLett.69.844](https://doi.org/10.1103/PhysRevLett.69.844)
- [9] L. N. Tong, M. H. Pan, J. Wu, X. S. Wu, J. Du, M. Lu, D. Feng, H. R. Zhai and H. Xia, "Magnetic and Transport Properties of Sputtered Fe/Si Multilayers," *The European Physical Journal B*, Vol. 5, No. 1, 1998, pp. 61-66. [doi:10.1007/s100510050419](https://doi.org/10.1007/s100510050419)
- [10] B. Briner and M. Landolt, "Intrinsic and Heat-Induced Exchange Coupling through Amorphous Silicon," *Physical Review Letters*, Vol. 73, No. 2, 1994, pp. 340-343. [doi:10.1103/PhysRevLett.73.340](https://doi.org/10.1103/PhysRevLett.73.340)
- [11] E. E. Fullerton, J. E. Mattson, S. R. Lee, C. H. Sowers, Y. Huang, G. Felcher and S. D. Bader, "Non-Oscillatory Antiferromagnetic Coupling in Sputtered Fe/Si Superlattices," *Journal of Magnetism and Magnetic Materials*, Vol. 117, No. 3, 1992, pp. L301-L306. [doi:10.1016/0304-8853\(92\)90084-2](https://doi.org/10.1016/0304-8853(92)90084-2)
- [12] A. Chaiken, R. P. Michel and M. A. Wall, "Structure and Magnetism of Fe/Si Multilayers Grown by Ion-Beam Sputtering," *Physical Review B*, Vol. 53, No. 9, 1996, pp. 5518-5529. [doi:10.1103/PhysRevB.53.5518](https://doi.org/10.1103/PhysRevB.53.5518)
- [13] K. Inomata, K. Yusu and Y. Saito, "Magnetoresistance Associated with Antiferromagnetic Interlayer Coupling Spaced by a Semiconductor in Fe/Si Multilayers," *Physical Review Letters*, Vol. 74, No. 10, 1995, pp. 1863-1866. [doi:10.1103/PhysRevLett.74.1863](https://doi.org/10.1103/PhysRevLett.74.1863)
- [14] E. G. Moroni, W. Wolf, J. Hafner and R. Podloucky, "Cohesive, Structural, and Electronic Properties of Fe-Si Compounds," *Physical Review B*, Vol. 59, No. 20, 1999, pp. 12860-12871. [doi:10.1103/PhysRevB.59.12860](https://doi.org/10.1103/PhysRevB.59.12860)
- [15] J. M. Gallego and R. Miranda, "The Fe/Si(100) Interface," *Journal of Applied Physics*, Vol. 69, No. 3, 1991, pp. 1377-1383. [doi:10.1063/1.347276](https://doi.org/10.1063/1.347276)
- [16] G. Creclius, "Reaction of Iron on Silicon," *Applied Surface Science*, Vols. 65-66, 1993, pp. 683-689. [doi:10.1016/0169-4332\(93\)90739-X](https://doi.org/10.1016/0169-4332(93)90739-X)
- [17] K. Konuma, J. Vrijmoeth, P. M. Zagwijn, J. W. M. Frenken, E. Vlieg and J. F. van der Veen, "Formation of Epitaxial β -FeSi₂ Films on Si(001) as Studied by Medium-Energy Ion Scattering," *Journal of Applied Physics*, Vol. 73, No. 3, 1993, pp. 1104-1109. [doi:10.1063/1.353273](https://doi.org/10.1063/1.353273)
- [18] E. V. Chubunova, I. D. Khabelashvili, Yu. Lebedinskii, V. N. Nevolin and A. Zenkevich, "Direct Observation of Silicide Growth at Fe-Si Interface during Pulsed Laser Deposition," *Thin Solid Films*, Vol. 247, No. 1, 1994, pp. 39-43. [doi:10.1016/0040-6090\(94\)90473-1](https://doi.org/10.1016/0040-6090(94)90473-1)
- [19] N. Cherief, J. Y. Veuillen, T. A. Nguyen Tan, R. Cinti and J. Derrien, "Formation of the Fe-Stepped Si(100) Interface as Studied by Electron Spectroscopy," *Vacuum*, Vol. 41, No. 4-6, 1990, pp. 1350-1352. [doi:10.1016/0042-207X\(90\)93954-H](https://doi.org/10.1016/0042-207X(90)93954-H)
- [20] J. M. Gallego, J. M. Garcia, J. Alvarez and R. Miranda, "Metallization-Induced Spontaneous Silicide Formation at Room Temperature: The Fe/Si Case," *Physical Review B*, Vol. 46, No. 20, 1992, pp. 13339-13344. [doi:10.1103/PhysRevB.46.13339](https://doi.org/10.1103/PhysRevB.46.13339)
- [21] J. Alvarez, J. J. Hinarejos, E. G. Michel, G. R. Castro and R. Miranda, "Electronic Structure of Iron Silicides Grown on Si(100) Determined by Photoelectron Spectroscopies," *Physical Review B*, Vol. 45, No. 24, 1992, pp. 14042-14051. [doi:10.1103/PhysRevB.45.14042](https://doi.org/10.1103/PhysRevB.45.14042)
- [22] S. R. Naik, S. Rai, G. S. Lodha and R. Brajpuriya, "X-Ray Reflectivity and Photoelectron Spectroscopy Study of Interdiffusion at the Si/Fe Interface," *Journal of Applied Physics*, Vol. 100, 2006, pp. 013514-013519. [doi:10.1063/1.2210168](https://doi.org/10.1063/1.2210168)
- [23] S. R. Naik, S. Rai, M. K. Tiwari and G. S. Lodha, "Structural Asymmetry of Si/Fe and Fe/Si Interface in Fe/Si Multilayers," *Journal of Physics D: Applied Physics*, Vol. 41, No. 11, 2008, pp. 115307-115312.

- [doi:10.1088/0022-3727/41/11/115307](https://doi.org/10.1088/0022-3727/41/11/115307)
- [24] G. J. Strijkers, J. T. Kohlhepp, H. J. M. Swagten and W. J. M. De Jonge, "Formation of Nonmagnetic c-Fe_{1-x}Si in Antiferromagnetically Coupled Epitaxial Fe/Si/Fe," *Physical Review B*, Vol. 60, No. 13, 1999, pp. 9583-9587.
[doi:10.1103/PhysRevB.60.9583](https://doi.org/10.1103/PhysRevB.60.9583)
- [25] J. F. Moulder, W. F. Stickle, P. E. Sobol and K. Bomben, "Handbook of X-Ray Photoelectron Spectroscopy," Perkin-Elmer, Eden Praire, 1995.
- [26] S. Hufner, "Photoelectron Spectroscopy," Springer, Berlin, 1995.
- [27] B. Dieny, P. Humbert, V. S. Speriosu, S. Metin, B. A. Gurney, P. Baumgart and H. Lefakis, "Giant Magnetoresistance of Magnetically Soft Sandwiches: Dependence on Temperature and on Layer Thicknesses," *Physical Review B*, Vol. 45, No. 2, 1992, pp. 806-813.
[doi:10.1103/PhysRevB.45.806](https://doi.org/10.1103/PhysRevB.45.806)
- [28] G. Marchal, Ph. Mangin and Ch. Janot, "Magnetism in Amorphous Fe-Si Alloys," *Solid State Communications*, Vol. 18, No. 6, 1976, pp. 739-742.
[doi:10.1016/0038-1098\(76\)91774-9](https://doi.org/10.1016/0038-1098(76)91774-9)